Applied Surface Science 367 (2016) 459–472

Contents lists available at ScienceDirect

Applied Surface Science

journal homepage: www.elsevier.com/locate/apsusc

Collector attachment to lead-activated sphalerite – Experiments and DFT study on pH and solvent effects

A. Sarvaramini[a], F. Larachi[a,*], B. Hart[b]

[a] Department of Chemical Engineering, Université Laval, 1065 Avenue de la médecine, Québec, Québec G1V 0A6, Canada
[b] Department of Earth Sciences, Surface Science Western, The University of Western Ontario, 999 Collip Circle, P.O. Box 12, London, Ontario N6G 0J3, Canada

ARTICLE INFO

Article history:
Received 7 December 2015
Received in revised form 22 January 2016
Accepted 24 January 2016
Available online 27 January 2016

Keywords:
Diisobutyl dithiophosphinate
Aerophine collector
Lead activation
Sphalerite
Flotation
DFT simulation
Solvent and pH effects
XPS

ABSTRACT

The interactions of diisobutyl dithiophosphinate with bare (un-activated) and lead-activated sphalerite were studied both experimentally and through DFT simulations. Sphalerite activated by lead in acidic and alkaline conditions showed considerably greater affinity for diisobutyl dithiophosphinate adsorption than bare sphalerite. Experimental observations supported by DFT simulations concur in that attachment of the solvated collector to the activated sphalerite surface is through adsorbed lead cations or lead hydroxides where as for the bare sphalerite, the collector was most stable in its solvated state and not as an adsorbed specie. Accounting for solvation effects by including a swarm of water molecules in DFT simulations was necessary to infer plausible surface interactions between collector, solvent, and bare or lead-activated sphalerite. The experimental data and DFT simulations indicate, affinity of the collector toward surface-adsorbed lead species was predicted to form stable covalent bonds between collector sulfur atoms and lead.

1. Introduction

Contamination of sulfide ores with lead is known to cause major problems in froth flotation processes [1–5]. For instance, inadvertent flotation of Pb^{2+}-contaminated sphalerite is a perennial challenge encountered during the flotation of complex galena-sphalerite ores. Lead contaminants could be sourced from recycled waters in the plant, from reagents such as lead acetates used during mineral treatment and processing, or merely liberated from lead-containing sulphide minerals such as galena [6,7]. Thiol collectors such as xanthates used for flotation of sulfide ores are known to adsorb directly on the galena surface unlike un-activated sphalerite which is known for its lack of affinity toward xanthate adsorption [8]. This could have led to a perfect textbook process to effortlessly separate galena from sphalerite in a flotation column. However, the presence of lead cations in the flotation pulp could be at the origin of a sphalerite lead-activation mechanism which would prompt collector adsorption on sphalerite, its flotation and consequently the presence of zinc impurities in the lead concentrate. Contamination of sphalerite by lead cations is documented in the literature to occur during different stages including mining, grinding and/or flotation and under wide ranges of pH from weakly acidic to alkaline media [6].

The mechanisms offered to explain sphalerite activation by lead, whether in acidic or alkaline conditions, are subject to considerable discrepancies in the literature. Following the paths for copper activation of sphalerite whereby copper cations replace zinc in the sphalerite lattice [9,10], an analogous exchange between lead cations at acidic pH and lattice zinc cations in sphalerite has been reported by several authors [11,12]. However, the possibility of exchange between lead cations and lattice zinc was rejected by Morey et al. [2] who compared cyclic voltammograms of lead-activated sphalerite and copper-activated sphalerite at pH 4.5. Voltammograms of Cu-activated sphalerite featured no reduction peak for copper species during the initial reduction step (cathodic sweep) supporting the depiction of adsorbed copper cation being incorporated into the ZnS lattice to form partially covalent sulfide species. Conversely, the reduction of Pb-activated sphalerite gave rise to a current peak at a voltage compatible with that observed from the reduction of Pb^{2+} adsorbed on a graphite surface immersed in a lead nitrate solution. Therefore, Morey et al. [2] concluded that, contrarily to the case of copper-activated sphalerite, the adsorption of Pb^{2+} on sphalerite precludes its further conversion into covalent lead sulfide species.

The lead-activation mechanism of sphalerite at pH >8 involves precipitation and adsorption of lead hydroxide species. According

* Corresponding author.
E-mail address: faical.larachi@gch.ulaval.ca (F. Larachi).

http://dx.doi.org/10.1016/j.apsusc.2016.01.213
0169-4332/

to Ralston et al. [13], a slow zinc to lead surface substitution takes place subsequently between $Pb(OH)_2$ and ZnS yielding $Zn(OH)_2$ precipitates on the sphalerite surface. However, no unanimity was reached in the literature regarding this latter substitution. Even if precipitation of lead hydroxide multilayers over the sphalerite surface was reported by Trahar et al. [12] in alkaline conditions, there was no evidence for surface exchanges between lead and lattice zinc. These authors concluded that sphalerite activation by lead at alkaline pH could only be due to the formation of lead hydroxide entities on the sphalerite surface.

Adsorbed lead cations and hydroxides on sphalerite surface are believed to be the active sites for the attachment of collectors. Formation of lead-ethyl xanthate chemical bonding in weakly acidic conditions was observed by Popov et al. [14] while studying infrared reflection spectra of lead-activated sphalerite in contact with potassium ethyl xanthate (KEX). Vucinic et al. [7] reported that adsorbed Pb^{2+} at pH 7 to 9.5 had a strong activation effect on the floatability of natural sphalerite and hypothesized formation of chemical bonding between lead and ethyl xanthate (EX) anions. The conjectured path consisted of an ion exchange between EX anions and OH^- groups adsorbed on the surface of adsorbed lead cations (Sph-Pb-OH) leading to the chemical adsorption of an ethyl xanthate monolayer (Sph-Pb-EX) on the surface of sphalerite. However, interactions of the collector with surface-exchanged lead cation (with sphalerite lattice zinc) were not excluded by Vucinic et al. [7] even though Trahar et al. [12] vouched for exclusive interactions between lead hydroxides and ethyl xanthate collector.

The goal of the present study is to investigate the interaction of diisobutyl dithiophosphinate collector with the lead activated sphalerite in acidic and alkaline media using experiments and density functional theory (DFT). Dialkyl dithiophosphinates are nonconventional collectors recommended in the flotation of sulphide ores containing copper, lead and precious metals from pyrite-rich minerals [15]. The low selectivity toward iron sulfides, such as pyrite, is thought to be the main advantage of these collectors over more conventional thiol-type collectors such as alkyl xanthates [16]. The interaction mechanism of diisobutyl dithiophosphinate collector (also known by its brand name as aerophine 3418) with un-activated pyrite [17,18] and galena [19] as well as copper-activated pyrite [17] has been investigated through cyclic voltammetry and surface analysis techniques to expose the chemical nature of the interaction between collector and the mineral's surface. However, the interaction of diisobutyl dithiophosphinate with lead-activated sphalerite in weakly acidic and alkaline pH is not well known in the literature and therefore this study constitutes an opportunity for generating new knowledge about this system. In addition, Although DFT is widely used in engineering to study the interaction, adsorption and reaction of different reagents in gas [20–22] and aqueous phase [23–26] with different nanoparticles, clusters and surfaces, the impact of presence of explicit water molecules as solvent in the adsorption mechanism, orientation and surface coverage in aqueous phase is neglected [23–26]. The presence of explicit water molecules in the simulation may lead to the considerable electron density shifting of the surface and reagent through the formation of different covalent and hydrogen bonding between the surface/reagent and water molecules which could alter the adsorption mechanism and energy. Although some efforts and computational expenses have been made to investigate the effect of solvent on the adsorption of the reagent on the surface, the numbers of explicit solvent molecules considered in the simulations have been too low to represent a real system [27,28]. Consequently, in this study we also try to address the importance of considering water molecules in the DFT simulations and we show how the DFT simulation could be in accordance with the experimental trends if we count on the presence of explicit water molecules in the simulations. In order to realize this study, the simulations have been performed in the presence of up to ninety water molecules in the slabs to simulate the existence of several layers of the solvents on the surface.

2. Experimental and computational methodologies

2.1. Materials

Sphalerite ore sample, provided by Ward's National Science, was sieved to remove particles coarser than 150 μm and finer than 90 μm. The elemental composition of the sample was obtained using atomic absorption spectrometry (AAS) showing the presence of Zn, S, Fe and Cu with the respective concentrations of 58 wt%, 31 wt%, 0.28 wt% and 0.07 mg/kg. The X-ray diffraction analysis of the sphalerite ore also revealed the presence of sphalerite, pyrite and silica with the respective proportions of 90 wt%, 4.7 wt% and 5.3 wt% calculated *via* the results of elemental analysis [29]. Prior to experiments, the oxide films on the sphalerite surface were removed by acid leach with HCl solution at pH = 2.

Distilled water was used for all the collector adsorption and flotation experiments. The reagents used in this study, lead nitrate, diisobutyl dithiophosphinate (aerophine 3418A, Cytec Canada), sodium hydroxide (97%, VWR international) and hydrochloric acid (Laboratoire Mat) were all with certified analytical grade.

2.2. Testing setup

Although the activity of diisobutyl dithiophosphinate for adsorption on the surface of different bare sulfide minerals such as pyrite, chalcopyrite and sphalerite as well as copper activated ores has been studied experimentally [30–32], no experimental work on its interaction with lead-activated sphalerite was found in the literature. Consequently, the affinity of this collector for adsorption on bare and lead-activated sphalerite in acidic (pH 4) and alkaline (pH 10) conditions was studied experimentally. A schematic of the experimental setup prepared to investigate the adsorption of diisobutyl dithiophosphinate and different lead species on the sphalerite surface is shown in Fig. 1. Lead nitrate solutions (150 mL at 1 mM at pH 4 and 10) were recirculated in a closed loop for *ca.* 30 min through a fixed-bed reactor containing 4 g of sieved sphalerite powder to allow lead species adsorption/precipitation on sphalerite. After this step, 70 mL of diisobutyl dithiophosphinate solution was passed through the sphalerite bed in a closed loop manner and the collector residual concentration was monitored using UV/Vis spectrophotometer. The decline of collector concentration in the solution demonstrated the activity of lead-activated sphalerite for diisobutyl dithiophosphinate adsorption. For the sake of comparison, the activity of unactivated sphalerite for the adsorption of diisobutyl dithiophosphinate was also investigated using the same setup.

As adsorption of both activation agent and collector on the sphalerite surface could influence its flotation recovery, microflotation tests were also performed to study the effects on sphalerite recovery resulting from collector adsorption and/or adsorption/precipitation of lead cation and hydroxide. The microflotation cell consisted of a cylindrical column 30 cm high and 1.7 cm inner diameter (Figure S1, supporting information). Prior to each experiment, 3 g of bare or pretreated sphalerite samples were loaded on the top of a fritted quartz disk (pore size <2 μm) acting as a gas distributor for the micro-flotation cell. Then 80 mL of diisobutyl dithiophosphinate solution (pH of 4 and 10) was added to the column where the particles were stirred using a magnetic stirrer placed atop of the porous disk. The flotation tests were started upon sparging, 37 mL/min of air, and the addition of 0.05 mL methyl isobutylcarbinol frother. The experiments were performed

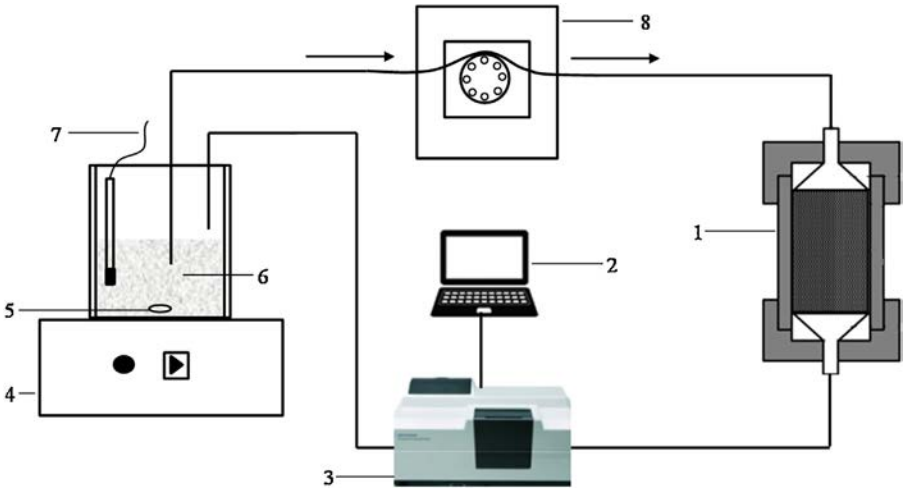

Fig. 1. Experimental setup used to study the activity of bare and Pb-activated sphalerite at alkaline and acidic pH for diisobutyl dithiophosphinate adsorption kinetics. 1. Fixed-bed reactor, 2. computer-controlled Cary WinUV software, 3. Cary 300 UV–visible spectrophotometer, 4. magnetic stirring plate, 5. magnetic stirrer, 6. activator/collector solutions, 7. pH-meter electrode, 8. peristaltic pump.

for 15 min and the concentrates were recovered by skimming the froth in the top bounder. The concentrates were subsequently washed, dried and weighted for quantifying the recovery of floated samples.

2.3. Surface analysis

To investigate the chemical state of different components on the surface of the samples recovered from the flotation experiments, X-ray photoelectron spectroscopy (XPS) analysis was performed on three different samples. The samples consisting of diisobutyl dithiophosphinate adsorbed activated sphalerite at alkaline pH (S1) and acidic pH (S2) and diisobutyl dithiophosphinate adsorbed bare sphalerite (S3) at alkaline pH. X-ray photoelectron spectra were acquired on an AXIS ULTRA spectrometer (Kratos Analytical) using Al monochromatic X-ray source operated at 300 W. Survey scans and high-resolution spectra for C 1s, O 1s, Zn2p, Zn-Auger, Pb4f and S2p were acquired using hybrid-mode lenses with 1 eV nominal resolutions (160 eV pass energy) and 0.1 eV (20–40 eV pass energy), respectively. Electrostatic charge appearing on the electrically insulating samples under X-ray irradiation was also neutralized with the integrated very low energy electron flood gun, the parameters of which are set to optimize energy resolution and counting rate.

2.4. Computational assumptions

Spin unrestricted DFT calculations were carried out for the total energy calculations and corresponding structure optimization to find the most stable geometries using DMol3 package implemented in Materials Studio 7.0. DMol3 applies numerical functions on an atom-centered grid as its atomic basis and atomic basis functions are attained by solving the DFT equations for every individual atom leading to rather accurate calculations. The Perdew–Burke–Ernzerhof generalized-gradient approximation (PBE) was used to approximate the exchange-correlation energy. The core electrons were treated using DFT semi-core Pseudopots and the double numerical plus d-function (DND) basis set was used to develop the electronic eigenstates with an orbital cut-off radius of 4.4 Å. The self-consistent field (SCF) convergence was fixed to 10^{-5} and the convergence criteria set for the energy, maximum force and maximum displacement were $2{\cdot}10^{-5}$ Ha, $4{\cdot}10^{-3}$ Ha/Å and $5{\cdot}10^{-3}$ Å, respectively.

Prior to the surface adsorption simulations, the sphalerite unit cell was optimized using DFT. The calculated sphalerite unit cell dimension was 5.47 Å which is only 1.1% larger than the experimental unit cell of sphalerite (5.41 Å). The optimized sphalerite unit cell was later used to cleave the (110) sphalerite plane which is its perfect cleavage plane and has been used as the principle sphalerite cleavage plane by different researchers for surface simulations [33–36]. The sphalerite surface was then modeled using (3×2) ZnS (110) surface supercell with 6 atomic layers slab and 30 Å vacuum spacing which resulted in a periodic cell of $16.4 \times 15.4 \times 39.6$ Å. The vacuum spacing was large enough to prevent interactions between image slabs. It is known that the sphalerite (110) surface undergoes considerable relaxation and reconstruction from the bulk termination [37–39]. Consequently, in all the simulations, the first 4 atomic layers were allowed to relax while the position of the atoms in the fifth and sixth layers was fixed to represent the bulk atoms of sphalerite. The interactions between collector, activation agents and water solvent with the sphalerite surface were simulated for a periodic cell of $16.4 \times 15.4 \times 39.6$ Å. Different configurations for the adsorption of collector and activator on the sphalerite surface were studied in terms of species (molecules, ions) relaxation on different surface adsorption sites and most stable configurations. In the absence of solvent, the adsorption energy of collector or/and activation agent on sphalerite was calculated as $E_{ads} = E_{[slab+reag]} - E_{[slab]} - E_{[reag]}$ where $E_{[slab+reag]}$ represents the total energy after reagent adsorption on the surface, $E_{[slab]}$ is the energy of relaxed bare slab and $E_{[reag]}$ is the energy of reagent molecule/ion. The calculated values for the adsorption energy of collector and activator on the sphalerite surface in the absence of solvent are tabulated and can be found in Table 1. Negative adsorption energy is indicative of exothermic adsorption and strong interaction of the collector/activator on the sphalerite surface. In the presence of solvent, first we obtained the total energy of the system consisting of the surface and the solvated reagent positioned far enough from the surface to prevent its adsorption. Then the solvated reagent was placed close to the surface in different configurations and the total system's energy was computed after adsorption on the solvated surface. The difference between the total energies whereby the reagent is adsorbed on the surface and where it is not adsorbed on the surface was obtained. Negative energy differences are an indication of favorable reagent adsorption on the surface in the solvated medium. A summary of the calculated

Table 1
Calculated adsorption energies of miscellaneous species (water, diisobutyl dithiophosphinate, Pb^{2+} and $Pb(OH)_2$) on un-activated and (Pb^{2+}/$Pb(OH)_2$) activated sphalerite in the absence of solvent.

Configuration	Adsorption energy (kJ/mol)
diisobutyl dithiophosphinate on un-activated sphalerite	−380.0
Pb^{2+} on sphalerite	−869.3
diisobutyl dithiophosphinate on Pb^{2+} activated sphalerite	−655.9
$Pb(OH)_2$ on sphalerite (monolayer average value)	−172.7
diisobutyl dithiophosphinate on $Pb(OH)_2$ activated sphalerite	−307.0

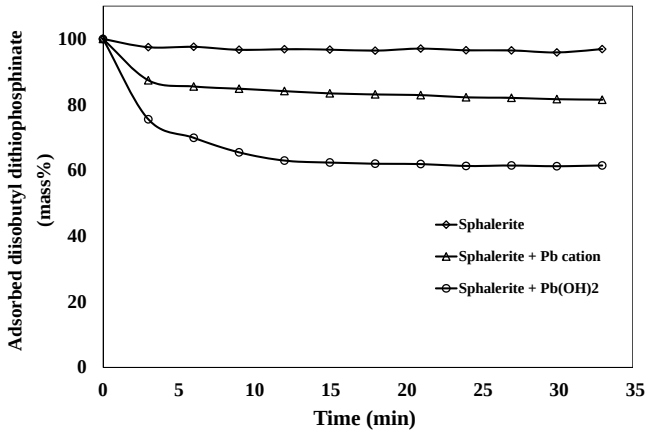

Fig. 2. Kinetics of diisobutyl dithiophosphinate adsorption on bare and lead-activated sphalerite.

energy differences due to the adsorption of different species on the surface in the solvated medium is presented in Table 2.

3. Results and discussion

3.1. Kinetics of diisobutyl dithiophosphinate adsorption on bare and activated sphalerite

Lead activation of sphalerite was performed both at acidic and alkaline pH. The presence of lead on the sphalerite surface after activation was confirmed through high-resolution XPS analysis. Lead concentration on the sphalerite surface treated at alkaline pH was 8.4% on surface atom basis. This concentration was significantly lower at acidic pH, *i.e.*, barely 1.1% of the sensed surface atoms. The main lead species to form at pH 10 and 4 are, respectively, $Pb(OH)_2$ and Pb^{2+} [40]. The higher surface Pb concentration at pH 10 could be due to the formation of a $Pb(OH)_2$ multilayer on the sphalerite surface. Coverage of non-porous sphalerite surface (surface area *ca.* 0.2 m^2/g) by a lead hydroxide monolayer was estimated to correspond to a surface concentration equal 8 μmol/m^2. This would be tantamount to an uptake of 0.2 mg of lead out of a solution initially loaded with 30 mg. Disappearance of turbidity after lead precipitation and its residual concentration in dissolved form falling below instrumental detection limits indicate that potentially a $Pb(OH)_2$ multilayer had formed on the surface of sphalerite particles. The unlikelihood of lattice replacement of zinc atoms by lead atoms was verified under acidic conditions by metal content analyses of the residual solutions after activation. Zinc went undetected in these solutions leading to the conclusion that the adsorption of lead cations or hydroxides on the sphalerite surface is the main contributor to Pb uptake.

Table 2
Change in total energy of the system due to adsorption of miscellaneous species (water, diisobutyl dithiophosphinate, Pb^{2+}) on un-activated and (Pb^{2+}/$Pb(OH)_2$) activated sphalerite in the presence of a solvating aqueous medium (positive values mean that total energy has increased).

Configuration	Adsorption energy (kJ/mol)
Solvated diisobutyl dithiophosphinate on un-activated sphalerite	+55.0
Solvated Pb^{2+} on sphalerite	−217.0
Solvated diisobutyl dithiophosphinate on Pb^{2+} activated sphalerite	−196.9
Solvated diisobutyl dithiophosphinate on $Pb(OH)_2$ monolayer formed on sphalerite	−182.1

Fig. 2 shows the kinetics of diisobutyl dithiophosphinate adsorption on the surface of bare and lead-activated sphalerite in acidic and alkaline conditions. The adsorption of diisobutyl dithiophosphinate, on the non-activated sphalerite was minimal as indicated by the limited, 4%, collector depletion from the solution after attaining adsorption equilibrium. Adsorption of diisobutyl dithiophosphinate on un-activated sphalerite could be attributed to the presence of lattice copper and iron impurities (see Section 2.1). Migration of copper impurities to the sphalerite surface, prompted by the initial acid washing pre-treatment, is indeed known to favor accretion of copper-containing deficient sulfide surface species which constitute by themselves self-activation sites [41]. Also, the presence of surface ferrous iron could activate the sphalerite surface through formation of collector-ferric hydroxyl complexes responsible for the minor adsorption of diisobutyl dithiophosphinate on bare sphalerite [9]. Remarkably, the lead-activated sphalerite exhibited much more pronounced affinity toward adsorbing the diisobutyl dithiophosphinate; up to 20% and 40% at acidic and alkaline pH, respectively (Fig. 2). Collector depletion from the solution was fast during the first 15 min then reaching equilibrium in almost 20 min. The higher adsorption of diisobutyl dithiophosphinate on the sphalerite sample treated at alkaline conditions could be due to higher amount of lead activation agents adsorbed on the sphalerite samples. However, apart from this study's proof that surface adsorbed lead cations and hydroxides develop an affinity for diisobutyl dithiophosphinate adsorption, no further effort was made to correlate the amount of adsorbed collector with the concentration of surface adsorbed/precipitated lead species.

As illustrated in Fig. 3, flotation tests have been carried out for un-activated/collector-free sphalerite, for lead-activated sphalerite and, for collector-adsorbed activated and un-activated sphalerite samples at pH 4 and 10. Recovery of bare sphalerite at pH 10 after 15 min of flotation amounted to *ca.* 67%. Such high recovery of bare sphalerite is comparable to that reported at close pH conditions by Hayes et al. [42], whom identified sulfur-rich and metal deficient hydrophobic mineral surfaces as well as the presence of copper ions in the sphalerite lattice as the main factors responsible for the high sphalerite recovery. According to Finkelstein and Stewart [43], even minute amounts of copper ions (as low as 0.04–.07 wt%) in the sphalerite lattice could have considerable effect on flotation recovery since copper inclusions are able to introduce surface acceptor levels into the zinc sulfide lattice [44]. Released electrons from oxidation of S^{2-} to elemental sulfur, be it *via* thermal agitation, could be

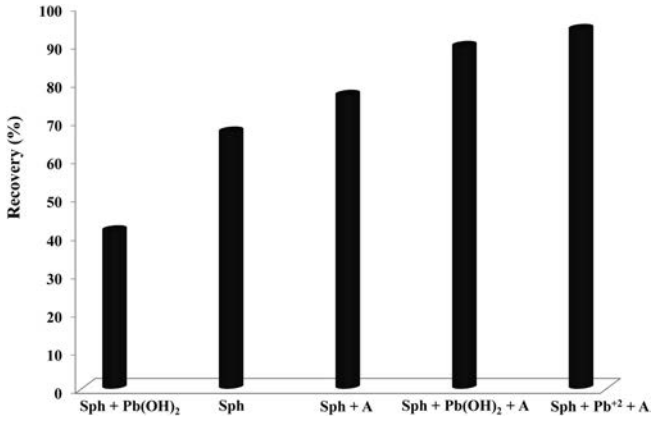

Fig. 3. Flotation recovery of bare and activated sphalerite (Sph) with and without aerophine collector (A).

transferred from the valence band to the acceptor level resulting into sulfur enriched sphalerite surface [44]. The presence of 0.05 wt% of copper within our sphalerite samples could hence be a reason for the high recovery of bare sphalerite. Likewise, oxidation of matrix iron (0.28 wt%) within or at the surface of the sphalerite could favor the formation of surface elemental sulfur contributing to the rise hydrophobicity and thus recovery of sphalerite [9]. After adsorption of diisobutyl dithiophosphinate, un-activated sphalerite shows noticeably higher recovery as compared to the flotation test with the bare sphalerite sample, *i.e.*, 77% *versus* 67% (Fig. 3).

Precipitation of $Pb(OH)_2$ on sphalerite surface at pH 10 led to an appreciable reduction of collector-less sphalerite recovery from 67% to 41% (Fig. 3). Such hydrophilic $Pb(OH)_2$ precipitate masks, through surface interactions with air bubbles, the native hydrophobic sphalerite surface sites. Reduction of collector-less sphalerite recovery due to nucleation and precipitation of lead hydroxides on sphalerite is in agreement with Rashchi et al. [6]. Adsorption of diisobutyl dithiophosphinate on the lead-activated sphalerite both at acidic and alkaline pH resulted in a considerably improved recovery of sphalerite, respectively, 90% and 94%. It is worthy of mention that these recoveries are comparable to those of ethyl-xanthate adsorbed lead-activated sphalerite reported by Trahar et al. [12] at acidic and alkaline pH.

3.2. Surface analysis

Elemental surface concentration from the XPS survey scans is shown in Table 3 for different sphalerite samples recovered after flotation: (S1) after collector adsorption on lead-activated sphalerite at alkaline pH, (S2) after collector adsorption on lead-activated sphalerite at acidic pH and (S3) after collection adsorption on bare sphalerite. Table 4 summarizes the photoelectron binding energies and relative contributions for carbon, lead, sulfur, oxygen and zinc in floated sphalerite samples (S1), (S2) and (S3). XPS analysis revealed the presence on the surface of *native* lead over the un-activated sample (S3) albeit in trace amounts. However, in agreement with the expected deposition of $Pb(OH)_2$ on the sphalerite surface, areal Pb atom percentage after alkaline activation exceeded by far that of (S2) and (S3) samples [12]. To gain insights on the chemical state of lead surface species, high-resolution Pb 4f core level spectra were also obtained and interference of Pb 4f and Zn 3s spectra was accounted for using a constrained curve fitting procedure (Figure S2, supporting information). Also, Table 4 summarizes the curve fitting results of the high resolution Pb 4f spectra for the three samples in terms of binding energies and relative contributions. The peak near 144 eV was assigned to Pb $4f_{5/2}$ and the location of Pb $4f_{7/2}$ was obtained considering a doublet separation of 4.86 eV with an intensity ratio of 1.33 for Pb $4f_{7/2}$/Pb $4f_{5/2}$. The binding energy (BE) of Pb$4f_{7/2}$ varied in a narrow range between 138.4 and 138.8 eV (Table 4). As lead sulfide gives rise to a lower BE peak near 137.4 eV, there is no indication for the exchange of lead with surface zinc and its integration during activation in the sphalerite lattice [45,46]. Rather, the Pb $4f_{7/2}$ binding energies are characteristic of lead oxides/hydroxides [47,48]. Also, exposure to CO_2 traces in air during flotation could also lead to the formation of lead carbonates for which the Pb$4f_{7/2}$ BE (138.6 eV) [49] is close to the BE range for our samples.

Oxygen contributed 30–40% of the surface elemental composition with a tendency of samples floated at alkaline pH to contain higher surface oxygen than those at acidic pH. For all three samples, the O 1s core-level spectra were fitted using 2 component peaks (Figure S3, supporting information). The lower BE component (530.6–531.1 eV) was assigned to chemisorbed oxygen or to hydroxyl groups at alkaline pH [50,51]. The contribution of this peak for lead-activated sphalerite at alkaline pH was considerably prominent due to $Pb(OH)_2$ precipitation. The O1s peak at higher BE (532.1–532.3 eV) was added to account for adsorbed water, and (frother) organic moieties and carbonate species on the sphalerite surface [50,52]. The presence of carbonate contamination was coherent with analysis of the high-resolution C 1s spectra of the 3 samples which were fitted using 3 components (Table 4 and Figure S4 in supporting information). The BE peak near 288–289 eV, especially prominent for sphalerite activated at alkaline pH, was attributed to surface adsorbed carbonates originating from the accelerated hydration of atmospheric CO_2 during the activation and flotation steps [45]. Finally, the aliphatic carbon signature characteristic of adsorbed diisobutyl dithiophosphinate contributed to inflate the peak contribution near 285 eV for S1–S3 samples.

For the sulfur chemical sate, the spectra were fitted using 1.18 eV doublet separations with 1:2 S $2p_{1/2}$ to S $2p_{3/2}$ intensity ratio. The binding energies for S $2p_{1/2}$ and S $2p_{3/2}$ components are reported in Table 4 and Figure S5 (supporting information) for the three samples. For each sample, two distinct S $2p_{1/2}$ and S $2p_{3/2}$ doublets were necessary to reconstruct the measured S 2p core-level spectra. The S $2p_{3/2}$ component with BE in the range 161.2–161.8 eV was attributed to S^{2-} in sphalerite [53–56] while the second S $2p_{3/2}$ component with BE near 162.3–162.7 eV was reminiscent of S_2^{2-} species [53–58]. The presence of S_2^{2-} vouches for the formation of sulfur–sulfur bonding on the sphalerite surface and suggests presumably sulfur enrichment due to oxidation [53]. The presence of iron impurities on the sphalerite surface could also favor formation of FeS_2 on the sphalerite surface. Nonetheless, the small excess noted on the abundances of S_2^{2-} form between lead-activated (S1 and S2) and non-activated (S3) sphalerite samples cannot be used as evidence for lead-promoted sphalerite surface oxidation.

Table 3
Apparent relative atomic percentages of various elements present in sphalerite samples recovered after flotation (S1) after adsorption of diisobutyl dithiophosphinate on lead-activated sphalerite at alkaline pH (S2) after diisobutyl dithiophosphinate adsorption on lead-activated sphalerite at acidic pH and (S3) after diisobutyl dithiophosphinate adsorbed on bare sphalerite.

Sample	Zn	Cu	O	C	S	Si	Mg	Pb	Fe
S1	11.9	0.72	38.8	23.2	11.8	1.9	1.0	8.4	2.1
S2	16.4	1.7	30.9	27.2	14.5	4.6	1.7	1.1	1.4
S3	13.6	1.0	41.7	20.5	11.0	7.3	2.2	0.56	2.1

3.3. DFT simulations

The following simulation aspects were developed in the sections below. First, the structures of diisobutyl dithiophosphinate were optimized with and without solvent. Relaxation of the cleaved

Table 4
Photoelectron binding energies and relative contributions for carbon, lead, sulfur, oxygen and zinc in sphalerite samples recovered after flotation (S1) after adsorption of diisobutyl dithiophosphinate on lead-activated sphalerite at alkaline pH (S2) after diisobutyl dithiophosphinate adsorption on lead-activated sphalerite at acidic pH and (S3) after diisobutyl dithiophosphinate adsorbed on bare sphalerite.

Sample	C 1s	Pb 4f	S 2p	O 1s	Zn 2p
S1	C 1s 285 eV (66.8%) C 1s 286.2 eV (15.4%) C1 s 289.0 eV (17.8%)	Pb $4f_{7/2}$ 138.4 eV (27.3%) Pb $4f_{5/2}$ 143.3 eV (20.5%) Zn 3s 139.9 eV (52.2%)	S $2p_{3/2}$ 161.6 eV (40.5%) S $2p_{1/2}$ 162.8 eV (20.2%) S $2p_{3/2}$ 162.6 eV (26.2%) S $2p_{1/2}$ 163.8 eV (13.1%)	O 1s 531.1 eV (53.7%) O 1s 532.1 eV (46.3%)	1021.5 (100%)
S2	C 1s 285 eV (80.1%) C 1s 286.2 eV (16.9%) C 1s 287.9 eV (3.0%)	Pb $4f_{7/2}$ 138.4 eV (4.2%) Pb $4f_{5/2}$ 143.2 eV (3.1%) Zn 3s 139.9 eV (92.7%)	S $2p_{3/2}$ 161.6 eV (42.4%) S $2p_{1/2}$ 162.8 eV (21.2%) S $2p_{3/2}$ 162.4 eV (24.3%) S $2p_{1/2}$ 163.6 eV (12.1%)	O 1s 531.1 eV (12.7%) O 1s 532.2 eV (87.3%)	1021.5 (100%)
S3	C 1s 285 eV (85.8%) C 1s 286.6 eV (9.2%) C 1s 288.7 eV (5.0%)	Pb $4f_{7/2}$ 138.8 eV (2.2%) Pb $4f_{5/2}$ 143.6 eV (1.6%) Zn 3s 139.9 eV (96.2%)	S $2p_{3/2}$ 161.7 eV (43.7%) S $2p_{1/2}$ 162.8 eV (21.8%) S $2p_{3/2}$ 162.3 eV (23.0%) S $2p_{1/2}$ 163.4 eV (11.5%)	O 1s 530.6 eV (10.8%) O 1s 532.3 eV (89.2%)	1021.6 (100%)

(110) sphalerite surface and reorganization of its surface atoms was then discussed. In two subsequent sections, the strength of adsorption on bare sphalerite of water molecules and of collector anions was simulated as a prelude to a section fully devoted to the mechanism of lead activated sphalerite for collector adsorption. The unlikelihood of substitution between adsorbed lead cations and lattice zinc atoms during lead activation of sphalerite was treated through DFT. Then, mechanisms of sphalerite activation *via* adsorption of solvated and non-solvated lead cations, *i.e.*, lead species prevailing in acidic conditions; followed by adsorption of solvated collectors on adsorbed lead cation were discussed. The whole simulation part was completed by DFT predicted scenario of the adsorption of lead hydroxides, *i.e.*, lead species prevailing in alkaline solutions, on the sphalerite surface and their potential role for the attachment of collectors.

3.3.1. Optimized structure of solvated collector

The molecular structure of collector plays an important role in its interaction with the surface of activated or un-activated sphalerite. Thus, the structures of diisobutyl dithiophosphinate were optimized through DFT simulations for different headspace environments. In absence of a solvation medium, the collector optimized structure (phosphorous atom bonded to two sulfur atoms and two isobutyl groups) is shown in Fig. 4a where the sulfur-phosphorous bond lengths are 2.017 and 2.020 Å, respectively. The electron from the negatively charged diisobutyl dithiophosphinate anion can be shared with the mineral surface through a covalent bond where valence electron transfer to the surface takes place from the collector highest occupied molecular orbital (HOMO). The composition of diisobutyl dithiophosphinate HOMO, illustrated in Fig. 4b, shows that the transferrable charge is located around the sulfur and phosphorous atoms. The $3p_x$ and $3p_z$ atomic orbitals of the two sulfur atoms have the most significant contribution to the collector HOMO with less considerable impact of phosphorous orbitals. Thus, the highest contribution to the collector covalent bonding with the mineral surface stems from its two sulfur atoms.

In the flotation process, diisobutyl dithiophosphinate is surrounded by water molecules which could influence its properties. Therefore, the effect of solvation on the electrical and geometrical properties of the collector was investigated through DFT by the relaxation of ninety water molecules around diisobutyl dithiophosphinate and the optimization of the solvated anion. The large size of diisobutyl dithiophosphinate anion due to the presence of two isobutyl groups necessitated implementation of ninety water molecules in the simulations to guarantee complete solvation of the collector in the slab. In addition, the number of water molecules around the collector anion was large enough so that addition of extra solvent molecules did not alter its properties after optimization. However, the excessive number of atoms involved in the simulations were computationally intensive so that water-collector assemblage was first optimized using classical force field-based simulation techniques. In this regard, the geometry of diisobutyl dithiophosphinate anion surrounded by ninety water molecules was optimized in the Forcite module of Materials Studio 7.0 using COMPASS as force field while the non-bond van der Waals and electrostatic interactions were set as atom-based summation method with a cut-of-radius equal 15.5 Å. The resultant optimized structure was then optimized using DFT resulting in a substantially reduced convergence time. The optimized structure of solvated diisobutyl dithiophosphinate along with the arrangements of water molecules around the collector anion is shown in Fig. 4c. The water molecules, while surrounding the collector, interact through hydrogen bonding with the sulfur atoms on the collector polar head. Though sulfur atoms are often weak hydrogen bond acceptors [59,60], each sulfur atom of the diisobutyl dithiophosphinate anion is seen to make up to three bonds with the hydrogen atoms of the surrounding solvent molecules. The hydrogen bond length between water molecules and sulfur atoms varies between 2.15 and 2.41 Å with an average length of 2.30 Å. Such interactions with solvent molecules led to changes in the collector electrical and geometrical properties. The electrons being shared through hydrogen bond contributed to reduce the negative charges around the sulfur atoms. The Mulliken atomic charge distribution of solvated diisobutyl dithiophosphinate showed slightly lower negative charges around sulfur atoms (average charge −0.77) than in the absence of water molecules (average charge −0.81). Such reduction forecasts a lowered electron donating ability in aqueous solution of diisobutyl dithiophosphinate. Also, reduction of the Van der Waals repulsive forces between the two sulfur atoms in the diisobutyl dithiophosphinate polar head leads to a reduced S═P═S angle: 115.88° in solvated form *versus* 121.39° in the absence of water molecules. Likewise, reduction of S═P═S angle led to an increase of isobutyl-P-isobutyl angle from 101.27° in vacuum to 104.926° for solvated collector. Furthermore, formation of hydrogen bond with water molecules tended to reduce the P═S bond strength. As a result, the average S═P bond length increased from 2.02 Å in vacuum to 2.05 Å under collector solvation.

3.3.2. Relaxation of (110) sphalerite surface

The DFT calculated surface energy of (110) surface is 0.37 J/m^2 which is about 42% lower than that of the unrelaxed (110) sphalerite surface. In the ideal sphalerite structure implemented in our electronic simulations, the (110) surface has the lowest surface energy and therefore is believed, owing to its highest stability, to be the most representative one for actual sphalerite mineral. The DFT simulation also indicated that the planar surface of sphalerite

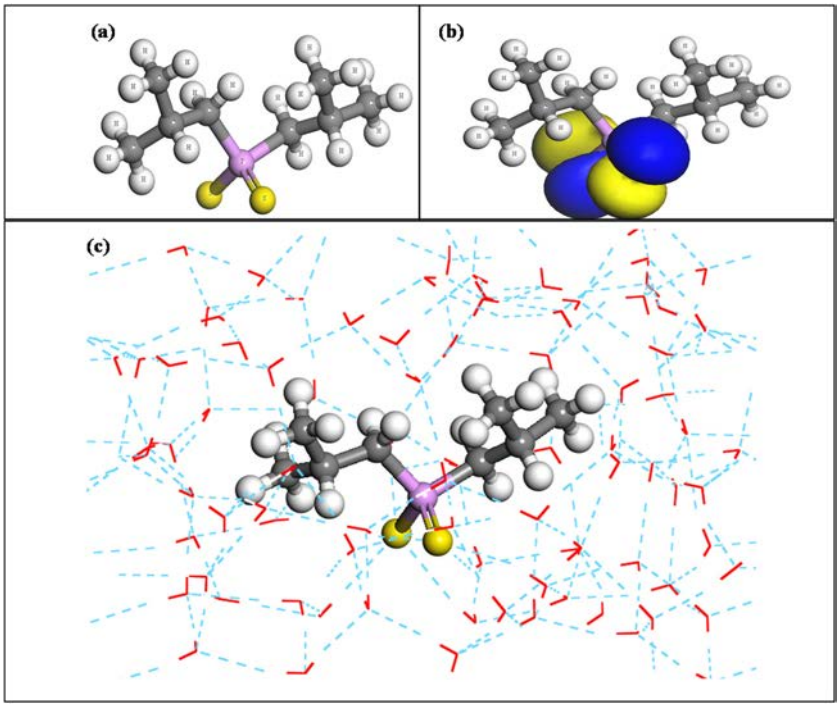

Fig. 4. DFT-optimized structure of non-solvated diisobutyl dithiophosphinate (a), highest occupied molecular orbital (HOMO) of non-solvated diisobutyl dithiophosphinate (b), DFT-optimized structure of diisobutyl dithiophosphinate solvated in the presence of 90 water molecules (c), (S ≡ Yellow, P ≡ Purple, C ≡ Gray, H ≡ White). (For interpretation of the references to color in this figure legend, the reader is referred to the web version of the article.)

(110) undergoes notable relaxation leading to parallel or normal displacements of Zn and S surface atoms with respect to their initial positions in uppermost layer (Fig. 5a and b). Displacements normal to (110) surface are more pronounced than those parallel to it and result in surface atoms to move outwardly by 0.13 Å and inwardly by 0.40 Å, respectively, for sulfur and zinc (Fig. 5c). These values are in close agreement with those estimated by Harmer et al. [39] from medium-energy ion scattering and XPS and by Duke et al. [37] from low-energy electron diffraction: 0.08 Å for S and −0.51 Å for Zn atoms in the first sphalerite (110) layer.

3.3.3. Adsorption of water on (110) sphalerite surface

Various initial positions for adsorption of water molecules on (110) sphalerite surface were considered leading in all cases to the same water adsorption configuration. The adsorption configuration of one single water molecule, shown in Fig. 6a, corresponds to the formation of a covalent bond between water O and surface Zn with 2.24 Å bond length, ∼47° tilt angle, and a computed adsorption energy of −93.5 kJ/mol. A larger water surface coverage was also simulated through the relaxation of 12 and 2 × 12 water molecules on the surface of a sphalerite 3 × 2 supercell with

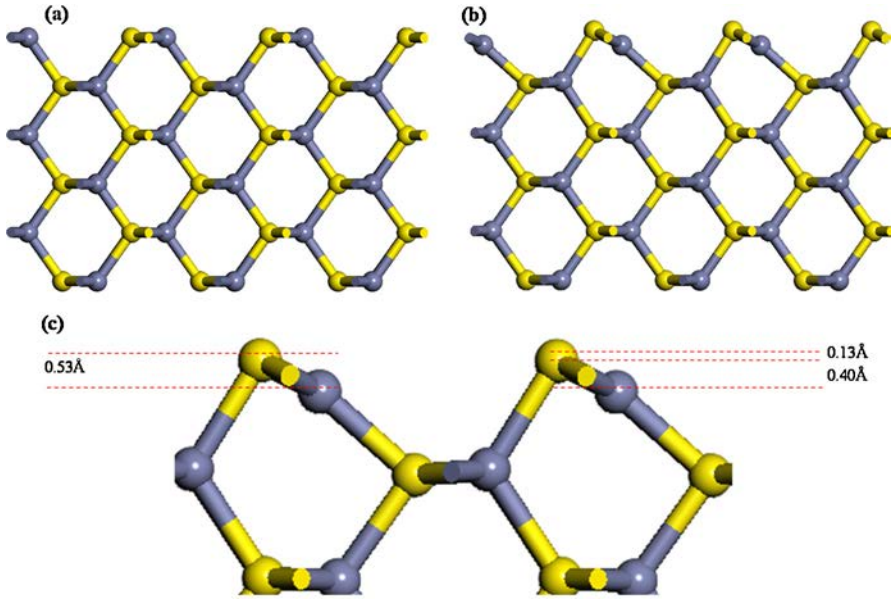

Fig. 5. Schematic of a six-layer (110) sphalerite slab after cleavage (a), sphalerite slab after relaxation (b), displacements of interfacial-layer Zn and S atoms after relaxation (c), (S ≡ Yellow and Zn ≡ Blue). (For interpretation of the references to color in this figure legend, the reader is referred to the web version of the article.)

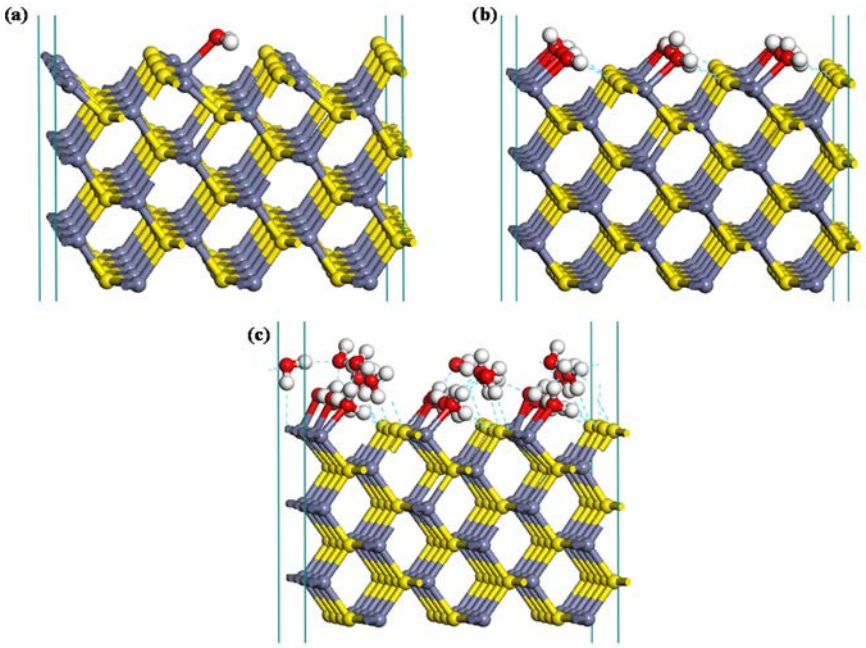

Fig. 6. Adsorption on (110) sphalerite (3 × 2 supercell) surface of 1 (a), 12 (b) and 24 water molecule(s) (c).

different combinations of initial positions. Consisting of 12 surface zinc atoms as electropositive adsorption centers, the supercell allowed adsorption of up to 12 water molecules. The most stable configuration arrived at by DFT simulation is shown in Fig. 6b where only 10 out of 12 H_2O molecules interacted with the surface through their oxygen atoms. The remaining molecules were left to adsorb on the surface through formation of hydrogen bonds (2.3 Å average length) with the covalently unsaturated surface sulfur atoms. The computed adsorption energy in the most stable configuration, −95.6 kJ/mol, was slightly lower than that for one single water molecule adsorbed on the surface. Flocking an increased number of water molecules near the surface is expected to reduce the average adsorption energy on account of augmented Van der Waals repulsion forces. On the contrary, in addition to non-covalently surface bonded H_2O molecules, formation of hydrogen bonds with surface sulfur atoms was also observed in the case of covalently bonded water molecules resulting in decreased water adsorption energy. The sphalerite supercell area, *ca.* 252.8 $Å^2$, has the potential to adsorb a water monolayer of more than twelve molecules (cross-section 7–8 $Å^2$/molecule) owing to many possible hydrogen bonds with the surface sulfur atoms. Hence, the most stable adsorption configuration with 24 water molecules consisted of up to 18 molecules adsorbed as a first monolayer. In this latter, 10 were adsorbed through covalent bonds between H_2O oxygen atoms and surface zinc atoms while the rest were adsorbed *via* formation of hydrogen bonds with sulfur atoms (Fig. 6c). The extra water molecules roofed the first monolayer by allowing hydrogen bonds with its adsorbed water molecules.

3.3.4. *Attachment of solvated collector on (110) sphalerite surface*

Two main adsorption configurations for diisobutyl dithiophosphinate on bare sphalerite surface are distinguishable as shown in Fig. 7a and b. In the most stable configuration (Fig. 7a), the collector adsorbed on the sphalerite surface through two covalent bonds between its sulfur atoms and two unsaturated *adjacent* surface zinc atoms located in the same row. The corresponding adsorption energy ranged between −370 and −380 kJ/mol depending on the rotation angle of the terminal methyl groups of the isobutyl branches around the S—P bonds. The average length of S—Zn covalent bond in this adsorption configuration is 2.38 Å. This is slightly higher than the S—Zn bond length of sphalerite crystalline structure (2.35 Å) and indicates the chemical bonding nature

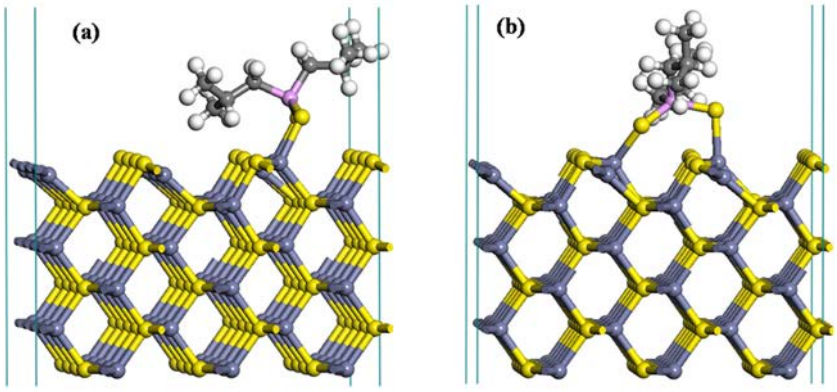

Fig. 7. Most stable adsorption configurations of diisobutyl dithiophosphinate on sphalerite surface in absence of solvent: two unsaturated adjacent surface zinc atoms located in same row (a), two unsaturated surface zinc atoms located in two different rows (b).

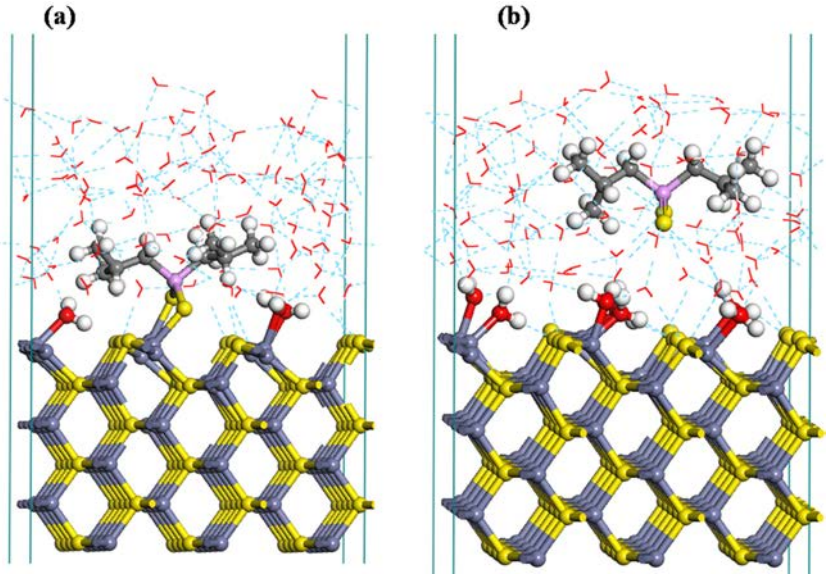

Fig. 8. Adsorption of solvated diisobutyl dithiophosphinate on sphalerite surface: most stable adsorbed configuration (a), non-adsorbed solvated collector (b).

of the interaction between collector and sphalerite surface. In the second most stable configuration (Fig. 7b), the collector established two covalent bonds with two unsaturated surface zinc atoms located in two *different* rows and distant by 5.4 Å. The corresponding adsorption energy, in the range −293 to −301 kJ/mol, was higher than when the collector involved two same-row adjacent zinc atoms only distant by 3.9 Å. Looser S—Zn bond lengths and lower stability adsorbed collector resulted due to a larger Zn–Zn distance. The S═P═S angle of adsorbed diisobutyl dithiophosphinate in first configuration (Fig. 7a) was 119°. This angle is close to equilibrium S═P═S angle of free diisobutyl dithiophosphinate (115.9°) unlike the lesser stability second configuration (Fig. 7b) for which the S═P═S angle was 126°. The adsorption energy of diisobutyl dithiophosphinate on un-activated sphalerite (110) surface is considerably lower than that reported by Liu et al. [34] for the adsorption of ethyl xanthate on a similar substrate which was −87.63 kJ/mol. Ethyl xanthate interacts indeed in a direction normal to sphalerite (110) surface by forming a covalent bond between the collector S atom and a surface zinc atom. However, bidentate adsorption of diisobutyl dithiophosphinate on un-activated sphalerite was always more favorable than monodentate adsorption. Analysis of the Mulliken charge density of diisobutyl dithiophosphinate and ethyl xanthate revealed that electron density around the sulfur atoms for the former slightly exceeded that around those of the latter collector portending stronger interaction of diisobutyl dithiophosphinate with surface zinc atoms.

The adsorption of solvated collector on the un-activated sphalerite was also studied through the relaxation of diisobutyl dithiophosphinate surrounded by 90 water molecules. The solvated collector was initialized at different locations on the sphalerite surface. The collector adsorption configuration with lowest total energy after relaxation is shown in Fig. 8a. However, the system's energy comprising surface adsorbed diisobutyl dithiophosphinate was always higher than when the solvated collector was not adsorbed on the sphalerite surface (Fig. 8b). Correspondingly, the number of water molecules adsorbed on the sphalerite surface was lower for the former than for the latter. This is tantamount to energy expenditure for bond breakage of some weakly bonded surface water molecules to allow adsorption of the *solvated* diisobutyl dithiophosphinate to occur. However, the energy released after collector adsorption was lower than the energy for water desorption from the surface. Consequently, solvated collectors far from the surface are always more stable than their configurations with adsorbed solvated collectors (+55 kJ/mol energy difference between adsorbed and non-adsorbed solvated collectors of Fig. 8a and b). Such lack of adsorption of diisobutyl dithiophosphinate on the surface of un-activated sphalerite was also observed through the experiments as detailed above (Fig. 2). This important finding stresses out the necessity to account in the DFT simulations for the presence of water molecules in order to arrive to meaningful predictions. Matter-of-factly, ignoring the presence of solvating molecules in the DFT simulations predicted energetically favorable adsorbed collector (Fig. 7) which was contradicted through experiments. Our results discourage the practice of ignoring solvation effect in the interpretation of the adsorption energies estimated by means of quantum mechanical simulations.

3.3.5. *Surface and bulk exchange of lattice zinc cations with lead cations*

Average exchange energy, E_{ex}, for replacement of zinc with lead cations is calculated as follows:

$$E_{ex} = \frac{E_{[slab+n\,Pb^{2+}]} + n\,E_{[Zn^{2+}]} - E_{[slab]} - n\,E_{[Pb^{2+}]}}{n} \quad (1)$$

In Eq. (1), n is the number of zinc cations replaced by lead cations, $E_{[slab+n\,Pb^{2+}]}$ is the total slab energy after substitution with n lead cations, $E_{[Zn^{2+}]}$ is the energy of a free zinc cation, $E_{[slab]}$ is the energy of the relaxed slab before Pb replacement and $E_{[Pb^{2+}]}$ is the energy of a free lead cation. The energy of free zinc and lead cations were obtained by first placing separately the lead and zinc atoms in a cell having the same size as the cell used in sphalerite relaxation calculations (16.4 × 15.4 × 39.6 Å) and then assigning +2 charge to the cell while implementing the same DFT parameters and convergence criteria used in all the DFT simulations.

The surface-exchanged lead cation after relaxation cannot but emerge out of the sphalerite surface as replacement of a zinc cation with a lead ion in the first layer leads to considerable deformation of the sphalerite surface (Figure S6a, supporting information). The resulting surface deformation could be due to the larger Van der Waals radius of lead (2.02 Å) in comparison to that of zinc (1.39 Å). The Pb—S bond length in the first sphalerite layer after relaxation is 2.73 Å which largely exceeds the bond length of Zn—S (2.28 Å) in sphalerite. Such large Pb—S bond length forced an outward movement of lead cation which while protruding on top of

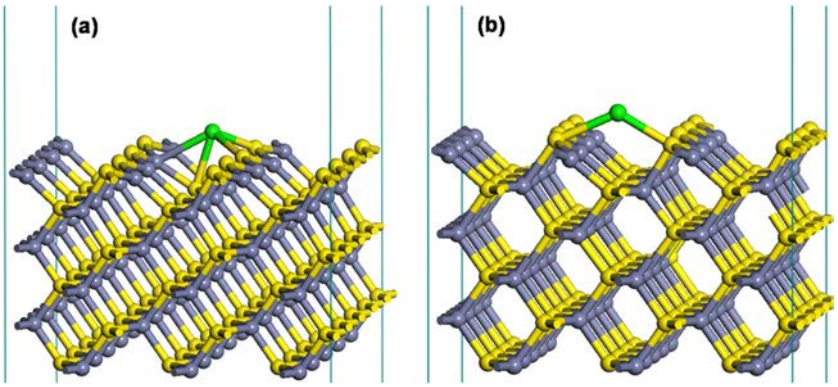

Fig. 9. The two energetically favorable adsorption configurations of lead cations on sphalerite surface: −869.3 kJ/mol (a), −837 kJ/mol (b).

the surface still remained part of the sphalerite lattice. However substitution of one zinc cation with lead on the first sphalerite layer is unfavorable on account of the computed exchange energy of +440 kJ/mol. Also, replacing all surface zinc cations with lead cations (Figure S6b, supporting information) even resulted in a larger average exchange energy of +518.4 kJ/mol. DFT simulation of further replacements involving the 2nd (bulk) layer of sphalerite was found to be even less energetically favorable (Figure S6c, supporting information). The considerable lattice distortions the intrusion of Pb^{2+} might impose to the bulk structure confirm the unlikelihood of lead cation diffusion to stabilize the sphalerite structure. Therefore, DFT simulations of the lead–sphalerite interactions clearly showed that direct exchange of lead with zinc on the surface or in the bulk of sphalerite is not energetically favorable and that Pb cations are incompatible with the sphalerite crystalline structure. Furthermore, these simulations are in agreement with the findings from our above described XPS results where no binding energy shift objectifying formation of PbS was observed from the spectra of the lead-activated sphalerite.

3.3.6. Adsorption of solvated collector on Pb^{2+}-activated sphalerite

For a study of the adsorption of Pb^{2+} on (110) sphalerite surface to reflect acidic conditions, the lead cations were located at five different initial positions: above surface S atoms, bridges between 2 same-row or 2 adjacent-row S atoms, hollows between sulfur and zinc atoms. As shown in Fig. 9, there are only two possible optimal configurations of Pb^{2+} adsorption on sphalerite surface. In the most stable configuration (Fig. 9a), lead cations adsorb while bridging 2 same-row unsaturated surface S atoms *via* two strong covalent bonds. Furthermore, the same Pb^{2+} ions are involved in weak covalent bond with saturated surface sulfur located in the second layer while sharing simultaneously electron density with a surface Zn cation (Fig. 9a). The adsorption energy of Pb^{2+} on the sphalerite surface in the most stable configuration is −869.3 kJ/mol and represents formation of strong covalent bonds between Pb^{2+} and sphalerite surface. A second adsorption configuration, though with a higher adsorption energy (−837 kJ/mol), is possible as shown in Fig. 9b where Pb^{2+} adsorbs through two covalent bonds with two unsaturated sulfur atoms located on two separate adjacent rows. The small difference between the adsorption energy of both configurations suggests that covalent bonds between Pb^{2+} and saturated sulfur or unsaturated surface zinc cations are weaker than those of Pb^{2+} with two unsaturated same-row or adjacent-row surface sulfur atoms.

Adsorption of diisobutyl dithiophosphinate on surface adsorbed lead cation was then simulated by locating the collector at different positions on top of the two previously identified stable adsorbed lead cations (Fig. 9). Only one stable adsorption configuration for diisobutyl dithiophosphinate adsorption on the adsorbed lead cation was obtained. Collector adsorption on the adsorbed lead cation occurs through formation of bidentate covalent bonding between the collector sulfur atoms and lead cation (Fig. 10a). This required breakage of one of the covalent bonds between lead and surface sphalerite sulfur. The average bond length of $S_{aerophine}$—Pb is 2.72 Å and is smaller than that of $S_{sphalerite}$—Pb (2.8 Å). Thus, the interaction between diisobutyl dithiophosphinate and lead cation is stronger than that of lead and sphalerite surface as confirmed from Mulliken charge calculations: −0.78e around collector sulfur atoms, *i.e.*, nearly thrice that around the sphalerite surface sulfur atoms (−0.26e). The angle of S=P=S of the diisobutyl dithiophosphinate molecule also decreases from 121.4° in equilibrium to 109.1° due to formation of bidentate bond between sulfur atoms and surface adsorbed lead cation.

The adsorption energy of diisobutyl dithiophosphinate on sphalerite surface can be estimated as:

$$E_{ads} = E_{[slab+Pb^{2+}+Aerophine]} - E_{[slab+Pb^{2+}]} - E_{[Aerophine]} \quad (2)$$

where $E_{[slab+Pb^{2+}+Aerophine]}$ is the total energy after adsorption of aerophine on the surface adsorbed lead cation, $E_{[slab+Pb^{2+}]}$ is the energy of the most stable configuration of adsorbed lead cation on sphalerite surface and $E_{[Aerophine]}$ is the energy of optimized diisobutyl dithiophosphinate free anion.

The adsorption energy of diisobutyl dithiophosphinate on lead cation was *ca.* −655.9 kJ/mol and vouches for the chemical nature of the bonding between aerophine and surface adsorbed lead cation. It is also almost twice the value obtained above for the adsorption of diisobutyl dithiophosphinate on the un-activated sphalerite surface (−380 kJ/mol), Fig. 7.

The solvating effect of water molecules on the adsorption of diisobutyl dithiophosphinate on Pb^{2+}-activated sphalerite was then studied by accounting for the presence of 90 H_2O molecules in the slab's overhead. The most stable Pb^{2+} form was the hydrate form $Pb(H_2O)_4^{2+}$ (Figure S7, supporting information) where the bonds between Pb^{2+} and water ligands are directed only toward part of the cation coordination sphere forming a hemi-directed coordination. The bond length between Pb^{2+} and water O varies between 2.47 Å to 2.76 Å.

Adsorption of the thus simulated solvated Pb^{2+} over surface of sphalerite was then studied through relaxation of the solvated cation on different surface locations. It can be seen from Figure S8 (supporting information) that adsorbed lead cation led to two covalent bonds with unsaturated surface S atoms similarly to the pattern reported above in the case of solvent-free adsorption (Fig. 9). The difference is more quantitative as the interaction of solvated lead cation with sphalerite surface is weaker than for the non-solvated cation reflecting in an average Pb—$S_{sphalerite}$ bond length of 2.93 Å

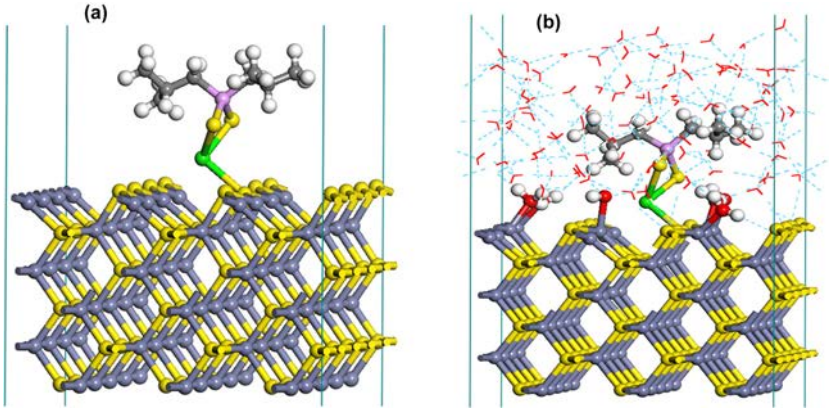

Fig. 10. Adsorption of diisobutyl dithiophosphinate on a surface Pb^{2+} adsorbed on sphalerite surface: non-solvated system (a), solvated system (b).

for the former as opposed to 2.8 Å for the latter. In addition, comparing the total energy of the systems consisting of surface adsorbed and non-adsorbed solvated lead cations showed that the adsorption of solvated lead cation only decreases the total system energy by −217 kJ/mol. However, as discussed earlier, the adsorption of non-solvated lead cation on the sphalerite surface decreases the total energy by −869.3 kJ/mol, revealing that the adsorption of lead cation on the sphalerite surface is less favored in a solvated medium. The adsorption of *solvated* Pb^{2+} necessitated that the two aqua-ligands with the largest bond length (2.76 Å and 2.65 Å) were to leave the coordination sphere of the solvated lead cation contributing thus in lowering its adsorption strength. Even though surface adsorbed solvated Pb^{2+} involved twice less solvent ligands than free solvated Pb^{2+}, adsorption of solvated lead cation was energetically favorable. The bond lengths between adsorbed Pb^{2+} and oxygen for the two remaining water ligands were 2.36 Å and 2.48 Å.

The interaction between adsorbed-solvated lead cation and solvated diisobutyl dithiophosphinate is depicted in Fig. 10b. The two covalent bonds between the two sulfur atoms of the collector and the surface adsorbed lead cation clearly show the finishing replacement of the two remaining water ligands bonded to lead cation. Furthermore, the lead cation sacrifices one of its covalent bonds with the surface sulfur atoms leading to the formation of a monodentate covalent bond between adsorbed lead cation and surface sulfur. Except the presence of water molecules, the adsorption configuration of the solvated diisobutyl dithiophosphinate on surface-adsorbed lead cation was similar to that predicted for the non-solvated collector (Fig. 10a). The decrease in total system's energy due to adsorption of the solvated collector on surface-adsorbed lead cation is −196.9 kJ/mol and pleads for an interaction between diisobutyl dithiophosphinate and the Pb^{2+} activated sphalerite overly estimated in the absence of solvent (adsorption energy of −655.9 kJ/mol). Finally, these DFT simulations confirm the affinity of surface adsorbed lead cation for prompting adsorption of solvated diisobutyl dithiophosphinate collector on Pb^{2+}-activated sphalerite in agreement with the experimental results discussed above.

3.3.7. Adsorption of solvated collector on $Pb(OH)_2$-activated sphalerite

$Pb(OH)_2$ as a predominant lead species at alkaline pH is likely to adsorb on sphalerite surfaces. As regards the computationally intensive simulations, these were restricted to analyze the formation of up to two lead hydroxide layers on the sphalerite surface. To identify the most energetically favorable monolayer adsorption configuration of lead hydroxide, different adsorption locations were initially tested. The most stable adsorbed monolayer $Pb(OH)_2$ configuration is shown in Fig. 11. Lead hydroxide monolayer is formed through participation of lead and an oxygen from $Pb(OH)_2$ to the formation of two covalent bonds, respectively, with surface S and Zn atoms. The bond lengths of Pb—S and O—Zn bonds are 2.78 Å and 1.99 Å, respectively. The second oxygen from lead hydroxide which did not participate to surface covalent bonding was involved in hydrogen bonding with hydrogen of an adjacent adsorbed lead hydroxide molecule. With a bond length of 1.74 Å, formation of O—H bonding between two adjacent $Pb(OH)_2$ contributed to stabilize the lead hydroxide monolayer. Similarly, an oxygen from $Pb(OH)_2$ and a lead cation from an adjacent $Pb(OH)_2$ were also shared as shown in the top view of Fig. 11b where oxygen-bridging enabled connecting two lead cations to each other. Furthermore, electron sharing between adjacent lead cations also appeared to contribute in the stabilization of the adsorbed lead hydroxide monolayer (Fig. 11b). This adsorption configuration was far more stable than other simulated configurations which resulted to the formation of stable monolayer of lead hydroxide consisting of twelve $Pb(OH)_2$ molecules. In order to obtain an average value for the adsorption energy of a $Pb(OH)_2$ molecule on the sphalerite surface in this configuration, the following equation was used:

$$E_{ads} = \frac{E_{[slab+Pb(OH)_2]} - E_{[slab]} - 12 * E_{[Pb(OH)_2]}}{12} \quad (3)$$

where $E_{[slab+Pb(OH)_2]}$ is the total energy after adsorption of a monolayer of $Pb(OH)_2$, $E_{[slab]}$ is the energy of relaxed sphalerite surface and $E_{[Pb(OH)_2]}$ is the energy of optimized $Pb(OH)_2$ free molecule.

Based on the above equation, the average adsorption energy per lead hydroxide molecule bonded to the surface was −172.7 kJ/mol. On top of the above hydroxide monolayer, addition of extra $Pb(OH)_2$ molecules led to the buildup of a second hydroxide layer. Formation of a second hydroxide layer took place through interlayer covalent Pb—Pb and Pb—O bonding in the respective ranges, [3.39–3.75 Å] and [2.31–2.63 Å] (Figure S9, supporting information). The average adsorption energy per adsorbed lead hydroxide molecule increased to about −132.2 kJ/mol. Here also, hydrogen bonding helped stabilizing the bilayer forming on the sphalerite surface. The most energetically favorable adsorption configuration of diisobutyl dithiophosphinate on top of a saturated sphalerite surface with $Pb(OH)_2$ monolayer is shown in Fig. 12. As can be seen, the collector adsorption took place through formation of covalent bonds between the collector S atoms and the Pb cations of $Pb(OH)_2$ monolayer. The adsorption energy for this configuration was about −307 kJ/mol and was higher than the adsorption energy of the collector on surface adsorbed lead cations (−655.9 kJ/mol), Fig. 10a.

Adsorption of diisobutyl dithiophosphinate on the $Pb(OH)_2$ monolayer could be affected by the presence of water molecules in the slab. The dominant mechanism for adsorption of one water molecule on the deposited lead hydroxide monolayer was

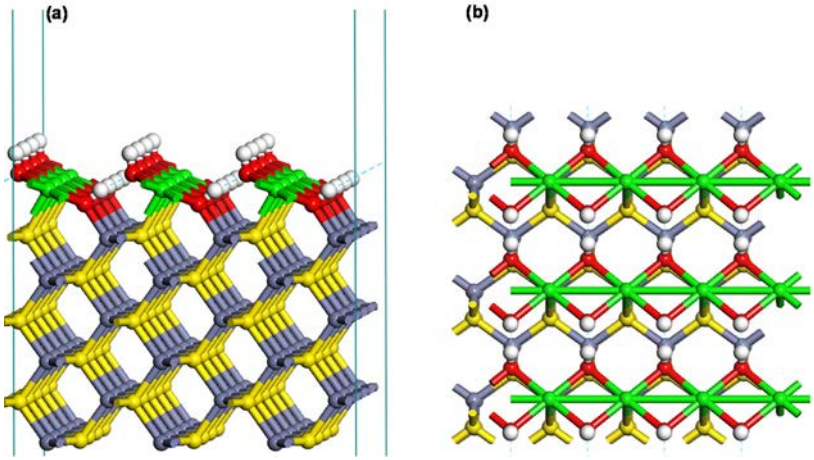

Fig. 11. The two energetically favorable adsorption configuration of lead hydroxide on (110) sphalerite surface: side view (a), top view (b).

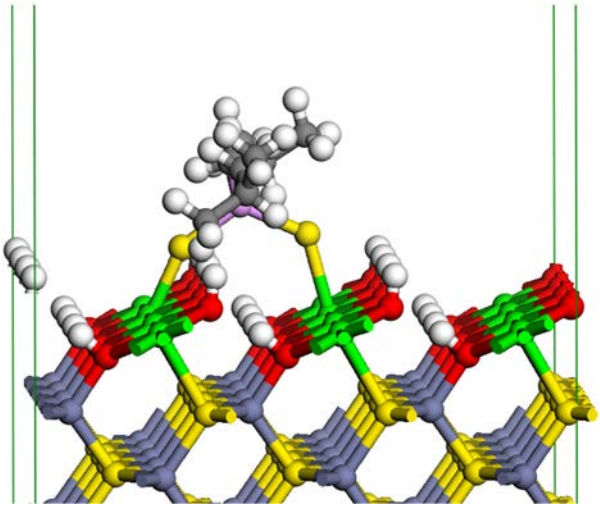

Fig. 12. Adsorption configuration of diisobutyl dithiophosphinate on the $Pb(OH)_2$ activated sphalerite.

through the physical adsorption and formation of hydrogen bonding between water molecule and the hydroxide group of $Pb(OH)_2$ as shown in Figure S10a (supporting information). The adsorption energy for one water molecule on a lead hydroxide monolayer is computed to be −71 kJ/mol. At higher surface water coverage, the average decrease in total energy per each adsorbed water molecule on the hydroxide monolayer is about −87.6 kJ/mol. Water adsorption on the lead hydroxide monolayer through formation of covalent bonding between O atom from H_2O and lead cation from hydroxides, was also observed at higher surface coverage (Figure S10b, supporting information). This resulted into lower average adsorption energy at higher coverage than for configurations where one water molecule is adsorbed. The average adsorption energy per water molecules on lead hydroxide was slightly higher than that of bare sphalerite (−95.6 kJ/mol). The solvating effect of water molecules on the adsorption of diisobutyl dithiophosphinate on $Pb(OH)_2$ activated sphalerite was studied considering the presence of 90 H_2O molecules in the slab. The collector adsorption configuration with lowest total energy after relaxation is shown in Fig. 13a. The total system's energy after collector adsorption on $Pb(OH)_2$ monolayer was −182.1 kJ/mol lower than the configuration with non-adsorbed collector (Fig. 13b) unveiling adsorption of diisobutyl dithiophosphinate on the $Pb(OH)_2$ activated surface an energetically favorable. The adsorption configuration of the solvated diisobutyl dithiophosphinate on surface deposited lead hydroxide was similar to that predicted for the non-solvated collector (Fig. 12). However, the calculated decrease in the total energy due to the adsorption of the solvated collector is −182.1 kJ/mol which is showing lower decrease than that of the non-solvated

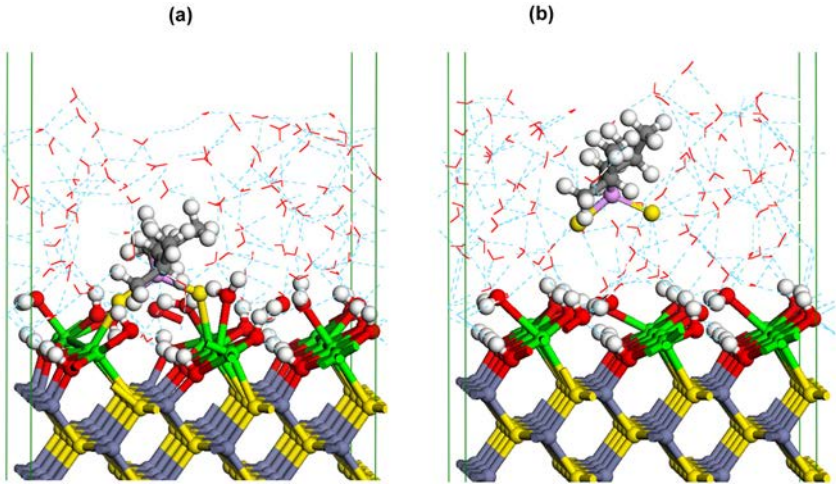

Fig. 13. Diisobutyl dithiophosphinate adsorption on $Pb(OH)_2$ activated sphalerite surface in the presence of water solvent: most stable configuration for the adsorption of solvated diisobutyl dithiophosphinate on the surface(a), solvated diisobutyl dithiophosphinate but non-adsorbed on the surface (b).

diisobutyl dithiophosphinate (−307 kJ/mol). In conclusion, these DFT simulations confirm the affinity of surface adsorbed lead cation for prompting adsorption of solvated diisobutyl dithiophosphinate collector on $Pb(OH)_2$ activated sphalerite in agreement with the experimental results deliberated earlier.

4. Conclusion

Lead activation of sphalerite and its interactions with diisobutyl dithiophosphinate collectors in alkaline and acidic conditions were systematically investigated both experimentally and through density functional theory (DFT) simulations to help elucidating the surface mechanisms arising during the inadvertent flotation of sphalerite. Adsorption of lead cations and lead hydroxides provided attractive sites for the collector attachment contrary to bare sphalerite which exhibited very low affinity toward the collector. The adsorption kinetics of diisobutyl dithiophosphinate on lead-activated sphalerite was quite rapid. Equilibrium was reached after 20 min while up to 40% of dissolved collector was adsorbed leading to >90% of activated sphalerite to be floated in a micro flotation column. Adsorbed collector and lead species on the sphalerite surface were objectified through the XPS analysis. No indications from surface analysis were in support of zinc cation substitutions by lead and sphalerite activation was likely induced through formation of surface adsorbed lead species. Unlikelihood of surface substitutions of lattice zinc cations with lead due to the latter's larger van der Waals radius and the significant lattice deformations exerted on the sphalerite structure was also concluded from DFT simulations. Solvated and non-solvated lead cations, *i.e.*, the dominant species at acidic pH, were shown to adsorb on the sphalerite surface by forming two covalent bonds with surface unsaturated sulfur atoms. The adsorbed lead cation in return was able to attach diisobutyl dithiophosphinate collector through the formation of two bidentate covalent bonds between the collector sulfur atoms and lead cation. However, the adsorption energy of both solvated Pb^{2+} and solvated collector were lower than when the effect of solvation was ignored. Attachment of diisobutyl dithiophosphinate was accompanied with the removal of covalent bonds between water molecules and adsorbed Pb^{2+} which was a phenomenon at the origin of the reduced diisobutyl dithiophosphinate adsorption energy. Lead hydroxide deposition on sphalerite, *i.e.*, occurring at alkaline pH, was shown to prompt formation of covalent bonding between lead and oxygen atoms of $Pb(OH)_2$, respectively, with surface sulfur and zinc atoms. Inception of hydrogen bonding among lead hydroxide molecules was shown to help stabilizing the deposited layer on the surface. In a similar manner, interactions of the collector with surface lead hydroxides took place *via* covalent bonds arising between the sulfur head of diisobutyl dithiophosphinate and the lead cations of $Pb(OH)_2$.

Acknowledgements

Financial support from the Natural Sciences and Engineering Research Council through its Cooperative Research & Development grants program and from the supporting partners Agnico Eagle, Barrick, Camiro, Corem, Glencore, IamGold, Niobec and Teck is gratefully acknowledged. We are also indebted to Compute Canada for the HPC platform without which the present DFT simulations would not have been possible.

Appendix A. Supplementary data

Supplementary data associated with this article can be found, in the online version, at http://dx.doi.org/10.1016/j.apsusc.2016.01.213.

References

[1] C.I. Basilio, I.J. Kartio, R.H. Yoon, Lead activation of sphalerite during galena flotation, Miner. Eng. 9 (1996) 869–879.
[2] M.S. Morey, S.R. Grano, J. Ralston, C.A. Prestidge, B. Verity, The electrochemistry of Pb^{II} activated sphalerite in relation to flotation, Miner. Eng. 14 (2001) 1009–1017.
[3] J.Y. Kim, S.L. Chryssoulis, Influence of lead ions in sulfide flotation – the application of laser-ionization mass spectrometry, Miner. Met. Process. 13 (1996) 69–76.
[4] C.C. Sui, S.H.R. Brienne, Z.H. Xu, J.A. Finch, Xanthate adsorption on Pb contaminated pyrite, Int. J. Miner. Process. 49 (1997) 207–221.
[5] P. Huang, M.L. Cao, Q. Liu, Selective depression of pyrite with chitosan in Pb–Fe sulfide flotation, Miner. Eng. 46–47 (2013) 45–51.
[6] F. Rashchi, C. Sui, J.A. Finch, Sphalerite activation and surface Pb ion concentration, Int. J. Miner. Process. 67 (2002) 43–58.
[7] D.R. Vucinic, P.M. Lazic, A.A. Rosic, Ethyl xanthate adsorption and adsorption kinetics on lead-modified galena and sphalerite under flotation conditions, Colloids Surf. A – Physicochem. Eng. Asp. 279 (2006) 96–104.
[8] A.R. O'Dea, K.E. Prince, R.S.C. Smart, A.R. Gerson, Secondary ion mass spectrometry investigation of the interaction of xanthate with galena, Int. J. Miner. Process. 61 (2001) 121–143.
[9] A.P. Chandra, A.R. Gerson, A review of the fundamental studies of the copper activation mechanisms for selective flotation of the sulfide minerals, sphalerite and pyrite, Adv. Colloid Interface Sci. 145 (2009) 97–110.
[10] A.R. Gerson, A.G. Lange, K.E. Prince, R.S. Smart, The mechanism of copper activation of sphalerite, Appl. Surf. Sci. 137 (1999) 207–223.
[11] J. Ralston, T.W. Healy, Activation of zinc-sulfide with Cu^{II}, Cd^{II} and Pb^{II}. 1. Activation in weakly acidic media, Int. J. Miner. Process. 7 (1980) 175–201.
[12] W.J. Trahar, G.D. Senior, G.W. Heyes, M.D. Creed, The activation of sphalerite by lead – a flotation perspective, Int. J. Miner. Process. 49 (1997) 121–148.
[13] J. Ralston, T.W. Healy, Activation of zinc-sulfide with Cu^{II}, Cd^{II} and Pb^{II}. 2. Activation in neutral and weakly alkaline media, Int. J. Miner. Process. 7 (1980) 203–217.
[14] S.R. Popov, D.R. Vucinic, J.W. Strojek, A. Denca, Effect of dissolved lead ions on the ethylxanthate adsorption on sphalerite in weakly acidic media, Int. J. Miner. Process. 27 (1989) 51–62.
[15] E.T. Pecina-Trevino, A. Uribe-Salas, F. Nava-Alonso, R. Perez-Garibay, On the sodium-diisobutyl dithiophosphinate (Aerophine 3418A) interaction with activated and unactivated galena and pyrite, Int. J. Miner. Process. 71 (2003) 201–217.
[16] T. Guler, Dithiophosphinate-pyrite interaction: voltammetry and DRIFT spectroscopy investigations at oxidizing potentials, J. Colloid Interface Sci. 288 (2005) 319–324.
[17] C. Hicyilmaz, N.E. Altun, Z. Ekmekci, G. Gokagac, Quantifying hydrophobicity of pyrite after copper activation and DTPI addition under electrochemically controlled conditions, Miner. Eng. 17 (2004) 879–890.
[18] C. Hicyilmaz, N.E. Altun, Z. Ekmekci, G. Gokagac, Pyrite-DTPI interaction as a function of pulp potential and pH, Colloids Surf. A – Physicochem. Eng. Asp. 233 (2004) 11–24.
[19] E.T. Pecina, A. Uribe, J.A. Finch, F. Nava, Mechanism of di-isobutyl dithiophosphinate adsorption onto galena and pyrite, Miner. Eng. 19 (2006) 904–911.
[20] D. Duzenli, D.O. Atmaca, M.G. Gezer, I. Onal, A density functional theory study of partial oxidation of propylene on $Cu_2O(001)$ and $CuO(001)$ surfaces, Appl. Surf. Sci. 355 (2015) 660–666.
[21] X. Wei, C. Dong, Z. Chen, K. Xiao, X. Li, Density functional theory study of SO_2-adsorbed Ni(111) and hydroxylated NiO(111) surface, Appl. Surf. Sci. 355 (2015) 429–435.
[22] G. Gomez, P.G. Belelli, G.F. Cabeza, N.J. Castellani, A theoretical view of 1,3-butadiene selective hydrogenation toward cis-2-butene on Pd–Ni layered catalyst, Appl. Surf. Sci. 353 (2015) 820–828.
[23] Y. Gilman, P.B. Allen, M.S. Hybertsen, Density-functional study of adsorption of isocyanides on a gold(111) surface, J. Phys. Chem. C 112 (2008) 3314–3320.
[24] W. Xiang, J. Liu, M. Chang, C. Zheng, The adsorption mechanism of elemental mercury on CuO (110) surface, Chem. Eng. J. 200 (2012) 91–96.
[25] S.K. Ramadugu, S.E. Mason, DFT study of antimony(V) oxyanion adsorption on α-Al_2O_3, J. Phys. Chem. C 119 (2015) 18149–18159.
[26] C. Zhao, J. Chen, Y. Li, D.W. Huang, W. Li, DFT study of interactions between calcium hydroxyl ions and pyrite, marcasite, pyrrhotite surfaces, Appl. Surf. Sci. 355 (2015) 577–581.
[27] A.P. Sandoval, J. Manuel Orts, A. Rodes, J.M. Feliu, Adsorption of glycine on Au(hkl) and gold thin film electrodes: an in situ spectroelectrochemical study, J. Phys. Chem. C 115 (2011) 16439–16450.
[28] J.N. Mills, I.T. McCrum, M.J. Janik, Alkali cation specific adsorption onto fcc(111) transition metal electrodes, Phys. Chem. Chem. Phys. 16 (2014) 13699–13707.
[29] A. Azizi, C.F. Petre, C. Olsen, F. Larachi, Untangling galvanic and passivation phenomena induced by sulfide minerals on precious metal leaching using a new packed-bed electrochemical cyanidation reactor, Hydrometallurgy 107 (2011) 101–111.
[30] V.A. Ignatkina, V.A. Bocharov, F.G. D'Yachkov, Collecting properties of diisobutyl dithiophosphinate in sulfide minerals flotation from sulfide ore, J. Miner. Sci. 49 (2013) 795–802.

[31] E.T. Pecina, A. Uribe, F. Nava, J.A. Finch, The role of copper and lead in the activation of pyrite in xanthate and non-xanthate systems, Miner. Eng. 19 (2006) 172–179.
[32] E.T. Pecina-Trevino, A. Uribe-Salas, F. Nava-Alonso, R. Perez-Garibay, Interaction mechanism of sodium diisobutylditiophosphinate with galena and pyrite, Afinidad 60 (2003) 246–252.
[33] J. Liu, S.M. Wen, X.M. Chen, S.J. Bai, D. Liu, Q.B. Cao, DFT computation of Cu adsorption on the S atoms of sphalerite (110) surface, Miner. Eng. 46–47 (2013) 1–5.
[34] J. Liu, S.M. Wen, J.S. Deng, X.M. Chen, Q.C. Feng, DFT study of ethyl xanthate interaction with sphalerite (110) surface in the absence and presence of copper, Appl. Surf. Sci. 311 (2014) 258–263.
[35] D.J. Simpson, T. Bredow, A.P. Chandra, G.P. Cavallaro, A.R. Gerson, The effect of iron and copper impurities on the wettability of sphalerite (110) surface, J. Comput. Chem. 32 (2011) 2022–2030.
[36] Y. Chen, J.H. Chen, J. Guo, Adsorption of O_2 and CN on the copper activated sphalerite (110) surface, Acta Phys. – Chim. Sin. 27 (2011) 363–368.
[37] C.B. Duke, R.J. Meyer, A. Paton, A. Kahn, J. Carelli, J.L. Yeh, Analysis of low-energy electron-diffraction intensities from ZnS(110), J. Vac. Sci. Technol. 18 (1981) 866–870.
[38] K. Wright, G.W. Watson, S.C. Parker, D.J. Vaughan, Simulation of the structure and stability of sphalerite (ZnS) surfaces, Am. Miner. 83 (1998) 141–146.
[39] S.L. Harmer, L.V. Goncharova, R. Kolarova, W.N. Lennard, M.A. Munoz-Marquez, I.V. Mitchell, H.W. Nesbitt, Surface structure of sphalerite studied by medium energy ion scattering and XPS, Surf. Sci. 601 (2007) 352–361.
[40] V.M. Nurchi, I. Villaescusa, The chemistry behind the use of agricultural biomass as sorbent for toxic metal ions: pH influence, binding groups and complexation equilibria, in: D. Matovic (Ed.), Biomass-Detection, Production and Usage, InTech, 2011, pp. 409–424.
[41] A.N. Buckley, R. Woods, H.J. Wouterlood, An XPS investigation of the surface of natural sphalerites under flotation-related conditions, Int. J. Miner. Process. 26 (1989) 29–49.
[42] R.A. Hayes, J. Ralston, The collectorless flotation and separation of sulfide minerals by Eh control, Int. J. Miner. Process. 23 (1988) 55–84.
[43] N.P. Finkelstein, B.V. Stewart, A preliminary investigation of the flotation of sphalerite without the use of collectors, National Institute of Metallurgy Report No. 1587, Johannesburg, South Africa, 1973.
[44] J. Ralston, P. Alabaster, T.W. Healy, Activation of zinc-sulfide with Cu^{II}, Cd^{II} and Pb^{II}. 3. The mass-spectrometric determination of elemental sulfur, Int. J. Miner. Process. 7 (1981) 279–310.
[45] Y.J. Peng, B. Wang, A. Gerson, The effect of electrochemical potential on the activation of pyrite by copper and lead ions during grinding, Int. J. Miner. Process. 102 (2012) 141–149.
[46] J. Liu, D.A. Aruguete, J.R. Jinschek, J.D. Rimstidt, M.F. Hochella, The non-oxidative dissolution of galena nanocrystals: insights into mineral dissolution rates as a function of grain size, shape, and aggregation state, Geochim. Cosmochim. Acta 72 (2008) 5984–5996.
[47] K. Laajalehto, R.S. Smart, J. Ralston, E. Suoninen, STM and XPS investigation of reaction of galena in air, Appl. Surf. Sci. 64 (1993) 29–39.
[48] G. De Giudici, A. Rossi, L. Fanfani, P. Lattanzi, Mechanisms of galena dissolution in oxygen-saturated solutions: evaluation of pH effect on apparent activation energies and mineral-water interface, Geochim. Cosmochim. Acta 69 (2005) 2321–2331.
[49] S. Lee, J.A. Dyer, D.L. Sparks, N.C. Scrivner, E.J. Elzinga, A multi-scale assessment of Pb(II) sorption on dolomite, J. Colloid Interface Sci. 298 (2006) 20–30.
[50] I.V. Chernyshova, S.I. Andreev, Spectroscopic study of galena surface oxidation in aqueous solutions. 1. Identification of surface species by XPS and ATR/FTIR spectroscopy, Appl. Surf. Sci. 108 (1997) 225–236.
[51] K. Laajalehto, P. Nowak, A. Pomianowski, E. Suoninen, Xanthate adsorption at PbS aqueous interfaces – comparison of XPS, infrared and electrochemical results, Colloid Surf. A – Physicochem. Eng. Asp. 57 (1991) 319–333.
[52] A.N. Buckley, R. Woods, An X-ray photoelectron spectroscopic study of the oxidation of galena, Appl. Surf. Sci. 17 (1984) 401–414.
[53] H.W. Nesbitt, L.J. Muir, A.R. Pratt, Oxidation of arsenopyrite by air and air-saturated, distilled water, and implications for mechanism of oxidation, Geochim. Cosmochim. Acta 59 (1995) 1773–1786.
[54] H.W. Nesbitt, G.M. Bancroft, A.R. Pratt, M.J. Scaini, Sulfur and iron surface states on fractured pyrite surfaces, Am. Miner. 83 (1998) 1067–1076.
[55] A.G. Schaufuss, H.W. Nesbitt, I. Kartio, K. Laajalehto, G.M. Bancroft, R. Szargan, Incipient oxidation of fractured pyrite surfaces in air, J. Electron Spectrosc. Relat. Phenom. 96 (1998) 69–82.
[56] A.G. Schaufuss, H.W. Nesbitt, I. Kartio, K. Laajalehto, G.M. Bancroft, R. Szargan, Reactivity of surface chemical states on fractured pyrite, Surf. Sci. 411 (1998) 321–328.
[57] M. Fujisawa, S. Suga, T. Mizokawa, A. Fujimori, K. Sato, Electronic structures of $CuFeS_2$ and $CuAl_{0.9}Fe_{0.1}S_2$ studied by electron and optical spectroscopies, Phys. Rev. B 49 (1994) 7155–7164.
[58] A.N. Buckley, R. Woods, The surface oxidation of pyrite, Appl. Surf. Sci. 27 (1987) 437–452.
[59] M.K. Shukla, J. Leszczynski, A theoretical study of hydration of 4-thiouracil in the electronic singlet excited state, Theochem – J. Mol. Struct. 771 (2006) 149–155.
[60] A. Yoshida, S. Shan, D. Herschlag, J.A. Piccirilli, The role of the cleavage site 2′-hydroxyl in the Tetrahymena group I ribozyme reaction, Chem. Biol. 7 (2000) 85–96.